

## Comparison between the electronic dielectric functions of a GaAs/AlAs superlattice and its bulk components by spectroscopic ellipsometry using core levels

O. Günther, C. Janowitz, G. Jungk, B. Jenichen, R. Hey, L. Däweritz, and K. Ploog  
*Paul-Drude-Institut für Festkörperelektronik, Hausvogteiplatz 5-7, D-10117 Berlin, Germany*

(Received 11 January 1995)

The dielectric functions of a GaAs/AlAs superlattice (SL) as well as its bulk constituents GaAs and AlAs were determined at  $T = 90$  K by means of spectroscopic ellipsometry with rotating analyzer using synchrotron radiation in the photon-energy range between  $3 \leq \hbar\omega \leq 25$  eV. This broad spectral range gives access to excitations from the Ga  $3d$  core levels lying approximately 20 eV below the conduction-band minimum. These levels are atomlike with virtually no dispersion throughout the Brillouin zone (BZ). They can thus be used as an energy reference to investigate confinement effects and level splittings on interband transitions in heterostructures compared to their bulk counterparts. The samples were grown by molecular-beam epitaxy and maintained under ultrahigh vacuum conditions from growth to measurement, avoiding the effects of cap or oxide layers, especially for AlAs. The investigation concerns transitions at  $L$ - and  $X$ -related points in the BZ which is tetragonal in the case of the SL and face-centered-cubic for the bulk samples. For the latter it is found that the  $L$ -related  $E_1$  structure consists of two spin-orbit-split groups of three transitions. For a  $(\text{GaAs})_m(\text{AlAs})_n$  SL with  $m = 9$ ,  $n = 7$  these two groups are blueshifted by about 200 meV compared with GaAs due to confinement effects. Similar shifts are not observed for transitions from the Ga  $3d$  levels to the conduction-band valleys. Therefore, the confinement acts on the highest valence bands. The major part of the SL  $E_1'$  structure is AlAs-like, but the minor one moves to higher energies by 165 and 80 meV compared to AlAs and GaAs, respectively. Since the two parts of the  $E_1'$  structure exhibit a different confinement behavior, they cannot have a common origin in  $\mathbf{k}$  space. The analysis of  $X$ -related  $E_2$  structures exhibits a blueshift for the SL transitions by about 55 meV compared with AlAs which is consistent with a confinement effect on the lowest conduction band. In correspondence to previous theoretical work a transition above the  $E_2$  critical point is found which was attributed to a SL specific transition due to the BZ folding. The comparison with the results for the bulk samples suggests a relation to the  $E_2(P_2)$  critical point. Beyond that, an analysis of the interband transition line shapes reveals for all  $E_1, E_1'$  structures, and the AlAs- $E_2$  one, that a modified Lorentzian profile indicating final-state interaction is more appropriate than two- or three-dimensional critical-point line shapes. This points to deviation from the one-electron band-structure picture even for transitions far above the fundamental absorption edge.

### I. INTRODUCTION

Semiconductor heterostructures and superlattices have attracted considerable attention because of intriguing electronic properties which are important for applications in optoelectronic devices. Most of the optical investigations have been restricted to the region near the fundamental absorption edge (for a review see Ref. 1). For comparison with band-structure calculations,<sup>2-4</sup> however, it is desirable also to know the optical properties well above the fundamental absorption edge.

Spectroscopic ellipsometry is a well-established method for obtaining the dielectric function of solids<sup>5,6</sup> and heterostructures<sup>7,8</sup> in a wide range of photon energies.<sup>9,10</sup> Ellipsometry measures the amplitude ratio of and the phase shift between the parallel and perpendicular polarized parts of the reflected light beam. From a single measurement we can therefore obtain two independent quantities which can be transformed into real and imaginary parts of the dielectric function in a straightforward manner. This is the major advantage of ellipsometry compared to other optical techniques, since the dielectric

function is closely related to the band structure.

Using ellipsometry we have studied similarities and differences between a short-period GaAs/AlAs superlattice (SL) and its bulk components in view of their optical properties and band structures. The  $(\text{GaAs})_m(\text{AlAs})_n$  SL's, with  $m$  and  $n$  indicating the number of monolayers, are prototypes of artificial heterostructures combining a direct-gap material with an indirect one. Because superlattices have a supercell in real space this leads to a folded Brillouin zone (BZ) in  $\mathbf{k}$  space<sup>11,12</sup> if the components of the SL have equivalent crystal structures and similar lattice constants. Within one superperiod of a GaAs/AlAs SL the Ga atoms are replaced by Al ones. In first order this results in a weak change of the total potential, which can be considered as the superimposed SL potential. The question is in which way the SL potential affects the electronic properties. Theoretical analysis for the band-gap region has revealed four types of GaAs/AlAs heterostructures,<sup>13</sup> classifying the behavior of the lowest conduction-band (CB) and highest valence-band (VB) states. The latter states are always confined to GaAs, but the  $\mathbf{k}$  localization of the states of the CB edge

varies for different values of  $m$  and  $n$ .  $(\text{GaAs})_m(\text{AlAs})_n$  SL's with  $n > 5$  have a direct gap in  $\mathbf{k}$  space. But in real space they change from having an indirect band gap for  $m < 7$  to a direct one for  $m > 9$ . SL's with intermediate  $m$  values have spectral strengths distributed between the two constituents concerning the bottom of the CB. We are not aware of similar detailed calculations with respect to other valence and conduction bands.

In this paper, we report on an experimental study of the effects of the SL potential on *higher* interband transitions, taking place at different locations in the BZ, and the influence of the final-state interaction. Additionally we are interested in whether we can observe transitions which are characteristic of a SL. The idea of using Ga 3*d* levels as an energy reference was realized in the following way (Figs. 1 and 2): For  $L$ - and  $X$ -related points the transitions from the Ga 3*d* levels to the lowest CB minima were analyzed for the GaAs bulk sample and then compared with those of the SL. This investigation probes the changes on the lowest CB due to the SL potential because the Ga 3*d* levels are almost not influenced by the superperiodicity. Then the observation of the interband transitions from the highest VB to the lowest CB yields the new behavior of the VB. In a further step, the changes on the second-lowest CB were investigated via the interband transitions from the highest VB.

The outline of this paper is as follows: In Sec. II we describe the model for the dielectric function which is the basis for the data evaluation. Section III deals with the experimental setup and the sample preparation. The results will be given in Sec. IV, and their discussion will follow in Sec. V.

## II. DIELECTRIC FUNCTION MODEL

The dielectric tensor reduces to a scalar function for the bulk samples with zinc-blende structure. The assumption of a cubic behavior of the dielectric function also for GaAs/AlAs superlattices, which is used

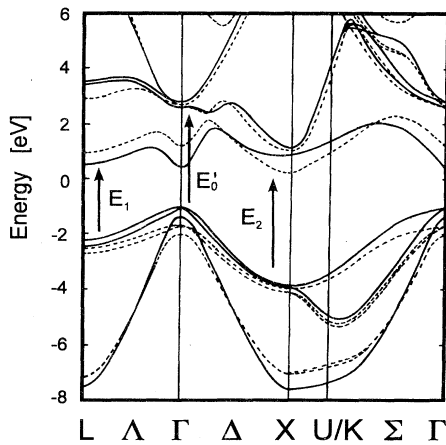


FIG. 1. LMTO band structure calculated within the LDA (Ref. 47) for GaAs (solid lines) and AlAs (dashed lines), plotted in one diagram to show energy differences at various points in the Brillouin zone.

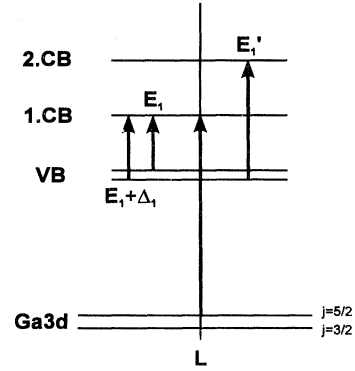


FIG. 2. Scheme of the investigated band-to-band transitions at the  $L$  point.

throughout this paper, represents a reasonable approximation within the investigated energy range, since the dielectric mismatch between GaAs and AlAs is small in the uv/vuv (vacuum ultraviolet) region.<sup>14</sup> The electronic dielectric function mainly includes contributions from vertical transitions in  $\mathbf{k}$  space, therefore depending merely on  $\omega$ . It contains the interband matrix elements  $P_{c,v}$ , the phenomenological broadening  $\Gamma$ , and the effects of the *joint* density of states (JDOS)  $J_{c,v}$ , combining the energy dispersion of the valence and conduction bands involved in the transition:<sup>15,16</sup>

$$\begin{aligned} \epsilon(\omega) = & 1 + \frac{\hbar^2 e^2}{\epsilon_0 m^2} \\ & \times \sum_{c,v} \int_0^\infty dE J_{c,v}(E) \left( \frac{|P_{c,v}|}{E} \right)^2 \\ & \times \left\{ \frac{1}{\hbar\omega + E + i\Gamma} - \frac{1}{\hbar\omega - E + i\Gamma} \right\}, \end{aligned} \quad (1)$$

with  $\epsilon_0$  the dielectric permittivity of the vacuum.

One can extract essential information about the dielectric function of crystalline materials using the concept of critical points,<sup>17,18</sup> which are defined by

$$\nabla_{\mathbf{k}}(E_c - E_v) = 0. \quad (2)$$

This relation is more likely fulfilled by energy bands at high-symmetry points or along symmetry lines. Assuming a constant matrix element for each critical point, it can be taken out of the integral. Structures in the dielectric function are then assigned to those of the joint density of states:

$$J_{c,v}(E) = \frac{2}{(2\pi)^3} \int_{E=E_c-E_v} \frac{dS}{|\nabla_{\mathbf{k}}(E_c - E_v)|}, \quad (3)$$

with  $dS$  the element of the constant energy surface  $E$ . Obviously, at critical points we expect singularities in the JDOS and therefore in the dielectric function. The matrix elements, depending on the symmetry of the wave functions, define the strength of the corresponding transitions. In the vicinity of a critical point, the  $E(\mathbf{k})$  expres-

sion is expanded in a Taylor series containing only the constant and quadratic terms. The nonresonant term in the curly bracket can be neglected in the case of derivative spectra of the dielectric function. Then the evaluation of the integral in Eq. (1) yields an analytic expression for  $\epsilon(\omega)$  which is used for the discussion of the line shapes [see Eq. (5)].

The JDOS approximation gives a reasonable physical model of the optical properties of crystals if deviations from the one-electron (band-structure) picture are not significant. Deviations may originate from the electron-hole interaction leading to excitons, from other many-particle excitations, or from the presence of disorder. A line-shape analysis of experimental data within this JDOS model of critical points yields quantitative values of the physical parameters (transition energy, oscillator strength, broadening) of the respective interband transitions as well as a clear indication of possible deviations from this model.

To emphasize the contributions originating from critical-point transitions, various modulation techniques have been developed.<sup>19</sup> The basic idea is their close relationship to a derivative of the measured quantity. However, the interpretation of the results is not straightforward since for the data evaluation a knowledge of the unmodulated quantity is necessary. In some cases, where the modulated quantity is related to higher-order derivatives, these techniques yield very sharp spectral features.<sup>20</sup> As a result of that, the determination of transition energies becomes quite accurate. The sharpening of spectral features gives a better chance to separate superimposed critical points which lie closely together on the energy scale.

Most of the drawbacks in modulation techniques can be overcome by means of precise measurements of the quantity of interest (e.g., dielectric function, reflectivity), followed by the numerical calculation of the required derivative with respect to photon energy. This procedure requires measurements with a high signal-to-noise ratio since every additional order of derivative will deteriorate this ratio. In practice, up to the second or third derivative acceptable signal-to-noise ratios are obtained using a proper experimental setup combined with an appropriate numerical data processing. Consequently, one takes more advantage of the experimental resolution capability if the line-shape analysis is applied to derivative spectra.

The experimentally determined ellipsometric angles (phase changes and amplitude ratios) are transformed into the dielectric function  $\epsilon = \epsilon_1 + i\epsilon_2$ , applying the most simple model with one surface and Fresnel's boundary conditions:<sup>21</sup>

$$\epsilon_1 + i\epsilon_2 = \epsilon_a \sin^2 \varphi_0 \left\{ 1 + \tan^2 \varphi_0 \left[ \frac{1 - \tan \Psi e^{i\Delta}}{1 + \tan \Psi e^{i\Delta}} \right]^2 \right\}, \quad (4)$$

with  $\varphi_0$  the angle of incidence,  $\epsilon_a$  the dielectric function of the ambient,  $\Psi$  the amplitude ratio, and  $\Delta$  the phase shift between the parallel and perpendicular polarized parts of the reflected light beam. This two-phase model is appropriate in our case due to the special sample preparation described below.

From the dielectric function data the second derivatives with respect to photon energy are calculated numerically. Then an extended form of the JDOS model of critical points allows a line-shape fit according to<sup>22,23</sup>

$$\frac{d^n \epsilon(\omega)}{d\omega^n} = A e^{i\phi} (\hbar\omega - E_{cp} + i\Gamma)^{-(n+1-d/2)}, \quad (5)$$

with  $\hbar\omega$  the photon energy,  $E_{cp}$  the critical-point energy,  $\Gamma$  the broadening parameter,  $d$  the k-space dimension of the critical point,  $\phi$  the excitonic phase, and  $A$  the amplitude of the critical-point transition. For the special values  $d = \phi = 0$ , Eq. (5) yields a Lorentzian line shape. Values of  $\phi = g\pi/2$ ,  $g$  integer, give the contribution from the one-electron band structure to the dielectric function within the JDOS model. Deviations due to many-particle effects, especially excitonic interaction, can be described by a metamorphism of van Hove singularities<sup>24</sup> performed mathematically by variation of  $\phi$ . Thus with one formula the JDOS model as well as excitoniclike line shapes are described.

### III. EXPERIMENTAL METHOD

The measurements for determining the photon-energy-dependent dielectric function were carried out under ultrahigh-vacuum conditions with a rotating analyzer ellipsometer using synchrotron radiation as a linearly polarized light source.<sup>25,26</sup> The base pressure in the ellipsometer was kept at  $1 \times 10^{-9}$  mbar. The spectral range of our equipment extends from 3 to 35 eV. Actually the high-energy limit depends on the reflectivity of the samples above the plasma edge and amounts to 25 eV in our case. This range covers the essential interband excitations as well as the transitions from the Ga 3*d* levels to the CB valleys. The energy resolution is better than 10 meV at 7 eV, and better than 60 meV around 20 eV. The resolution of the ellipsometric setup is limited by the higher light intensity requirements compared to a reflectivity experiment. The samples were mounted under vacuum conditions onto a Cu sample holder, which was cooled with liquid nitrogen.

We have extensively studied three samples, a GaAs and an AlAs layer as well as a GaAs/AlAs SL. Both the GaAs and AlAs layers were 500 nm thick. The (GaAs)<sub>*m*</sub>(AlAs)<sub>*n*</sub> SL consisted of 100 periods of  $m = 9$  and  $n = 7$  ML resulting in a total layer thickness of about 500 nm, too. We have chosen the (GaAs)<sub>9</sub>(AlAs)<sub>7</sub> SL as a good compromise in view of maintaining the SL property but accumulating enough monolayers in order to establish bulklike electronic properties in each constituent layer. Moreover, to get simple tetragonal symmetry of the SL BZ (Ref. 11) we choose the sum  $m + n$  to be even.

All samples were grown by MBE on rotating semi-insulating (001) GaAs substrates at  $T = 550^\circ\text{C}$  with an additional 500-nm GaAs buffer layer and were undoped. After growth the samples were transported without breaking the ultrahigh-vacuum conditions from the molecular-beam-epitaxy (MBE) equipment to the UHV ellipsometer at the synchrotron radiation source BESSY I, Berlin. All samples have got surfaces as grown, i.e., As terminated, thus avoiding difficulties with additional cap

layers, oxidized surfaces, etc. We are thus able to compare precisely the dielectric function of the SL with the bulk properties of its components, including the extremely oxygen-sensitive AlAs. By means of such vacuum-based experiments the surface preparation is exactly equivalent throughout all samples.

#### IV. EXPERIMENTAL RESULTS

Figure 3 shows the imaginary parts of the dielectric function for the SL and the bulk samples in the energy region from 3 to 9 eV. Each sample exhibits three main structures which are related to three major contributions to the JDOS. They are denoted by  $E_1$ ,  $E_2$ , and  $E'_1$ ,<sup>27</sup> and constitute a common feature of the group-IV semiconductors as well as of the compound III-V and II-VI semiconductors. The  $E_2$  and  $E'_1$  structures have almost the same energy position for all samples. The  $E_2$  peak is located between 4.5 and 5 eV, and the  $E'_1$  structure lies around 6.5 eV. In contrast, it is obvious from Fig. 3 that the energy positions of the  $E_1$  structure of GaAs and the SL sample are very similar, whereas the corresponding structure of AlAs lies by 1 eV at higher energies. The SL  $E_1$  structure is shifted to higher energies by more than 200 meV as compared to GaAs.

The derivative spectra in Fig. 4 reveal that the  $E_1$  structure of each sample consists of two groups of three separate transitions. The energy separation between these two groups is due to spin-orbit splitting of the uppermost valence band and amounts to 0.211 eV for GaAs and 0.169 eV for AlAs. Each group has its main structure on the high-energy side. The separation between the transitions of each group is almost constant for a considered sample and has a value of  $75 \pm 5$  meV for GaAs,  $49 \pm 5$  meV for AlAs, and  $102 \pm 3$  meV for the SL.

In Fig. 5 the corresponding derivative spectra for the  $E_2$  structure are shown. The spectra for AlAs and the SL are very similar, and show two strong and sharp minima,

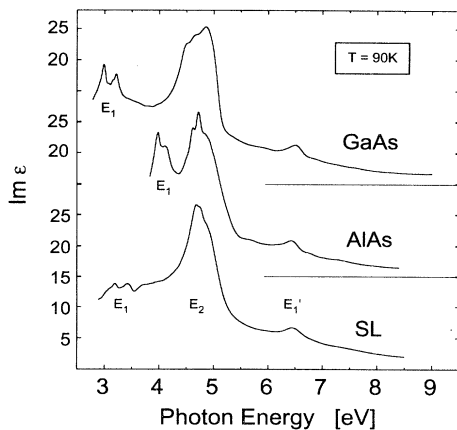


FIG. 3. Imaginary part of the dielectric functions for the bulk GaAs and AlAs samples and for a  $(\text{GaAs})_9/(\text{AlAs})_7$  superlattice. The three characteristic structures  $E_1$ ,  $E_2$ , and  $E'_1$  in each of these spectra correspond to transitions at critical points.

which are shifted by about 55 meV to higher energies in the case of the SL compared to AlAs. The separation between these two transitions amounts to 95 meV for AlAs and 90 meV for the SL. Additionally, at an energy of 4.953 eV the derivative spectrum for the SL sample exhibits one further prominent minimum, which corresponds to a shoulder in the original spectrum of the dielectric function. The derivative spectrum for GaAs differs in shape from those of AlAs and the SL, and exhibits four broad minima which are denoted by  $E'_0$ ,  $E_2(X)$  and  $E_2(P_2)$  with increasing energy.

The spectra of the dielectric function in the vicinity of the  $E'_1$  critical point (Fig. 6) exhibit for all samples one main peak around 6.5 eV accompanied by a smaller structure on the high-energy side. These are denoted by  $E'_1$ . The energy separation between the two structures amounts to 0.317 eV for GaAs and 0.335 eV for AlAs. Additional weaker structures are found for all samples at lower energies, just below 6 eV, as well as at the high-energy side above 7 eV. The energy position of the main  $E'_1$  peak is almost the same for AlAs (6.475 eV) and the

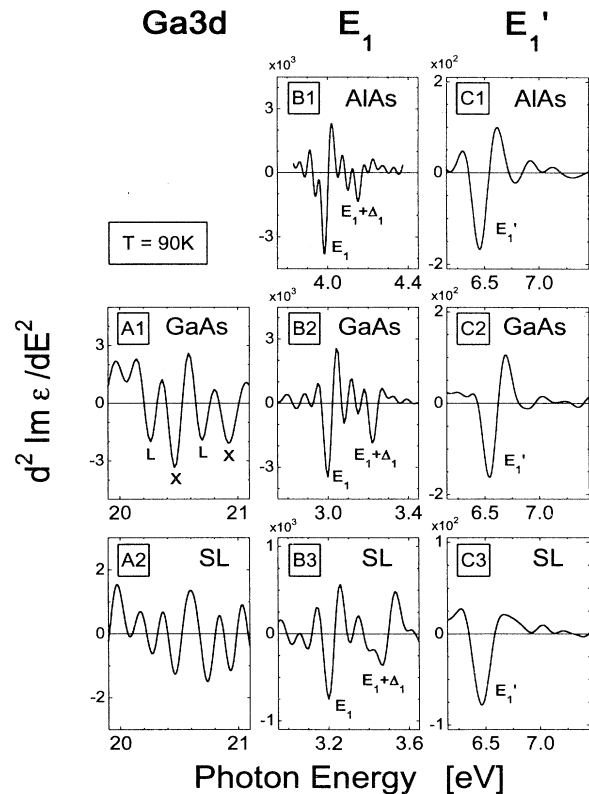


FIG. 4. Second derivatives of the imaginary part of the dielectric function vs photon energy for the Ga 3d- and L-related band-to-band transitions for GaAs, AlAs, and the  $(\text{GaAs})_9/(\text{AlAs})_7$  superlattice: (A) The Ga 3d transitions to the conduction-band minima at L- and X-like points in the BZ exhibit no shifts in transition energies for the superlattice compared to GaAs. (B) Blueshift of the  $E_1$  transitions by 200 meV for the superlattice compared to GaAs. (C) The major part of the  $E'_1$  structure for the superlattice is an AlAs-like transition.

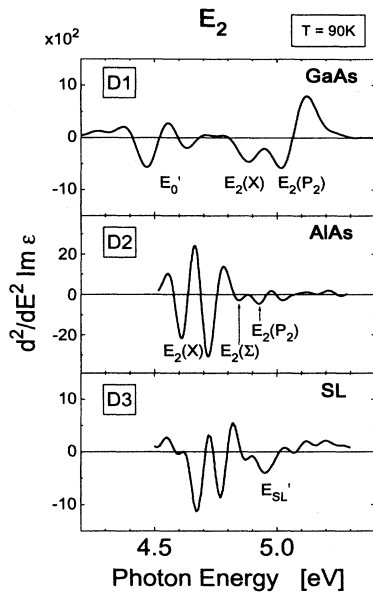


FIG. 5. The comparison of transition energies, commenced in Fig. 4, is continued here for the  $X$ -related interband transitions: (D) The second derivatives of the imaginary part of the dielectric function for GaAs, AlAs, and the  $(\text{GaAs})_9(\text{AlAs})_7$  superlattice. The minima are denoted by the corresponding critical points. The shape of the superlattice spectrum is AlAs like but shifted by 55 meV to higher energies. For a discussion of the  $E_{\text{SL}}$  structure (Ref. 50), see text.

SL (6.470 eV), whereas the corresponding peak of GaAs lies at 6.578 eV. The minor part of the  $E'_1$  structure of the SL is shifted to higher energies by 165 and 80 meV compared to that of AlAs and GaAs, respectively.

In the energy range from 19 to 24 eV we observe two broad peaks in the spectrum of the dielectric function (Fig. 7). The onset of the first peak corresponds to the lowest excitations with respect to energy from the quasi-

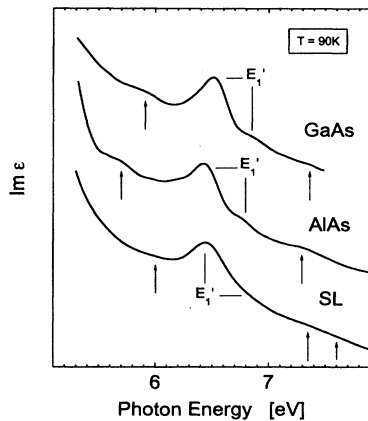


FIG. 6. Imaginary part of the dielectric function in the vicinity of the  $E'_1$  structure showing additional transitions (denoted by the arrows) at the low- and high-energy sides.

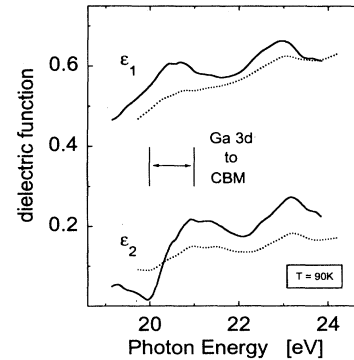


FIG. 7. Dielectric function vs photon energy in the region of the transitions from the Ga 3d core levels to the lower conduction bands for the GaAs bulk sample (solid line) and a  $(\text{GaAs})_9(\text{AlAs})_7$  superlattice (dotted line). For the two main peaks of GaAs, even in this nondervative spectrum, a fine structure has been resolved which is related to transitions to the conduction-band minima at  $L$  and  $X$  in the marked region between 20 and 21 eV.

dispersionless Ga 3d levels to the CB minima. Even in the nondervative spectrum we resolve a fine structure which is related to the spin-orbit splitting, lifting the degeneracy of the Ga 3d levels. For the GaAs bulk sample we found a splitting value of  $0.44 \pm 0.03$  eV. As expected, the value for the SL is similar and amounts to  $0.46 \pm 0.03$  eV. The derivative spectrum of the imaginary part of the dielectric function for GaAs, shown in Fig. 4, clearly exhibit four main minima, which also appear in the case of the SL sample at virtually the same energy positions. Thus the comparison of the SL spectrum with that of the bulk GaAs sample reveals no shifts or splittings in these transitions.

Line-shape fits using Eq. (5) were performed for all observed interband transitions. The determined transition energies are compiled in Table I. The aim of these line-shape fits is twofold: First, the quantitative values obtained for the interband transition parameters easily enable a comparison between different investigations. Second, the limits of the one-electron picture can be explored. For this latter reason comparative line-shape fits were performed according to two- or three-dimensional critical points and modified Lorentzian resonances. For most interband transitions (all  $E_1$  and  $E'_1$  structures and the AlAs  $E_2$  one) at  $T = 90$  K we find that the modified Lorentzian profile, which is characteristic of final-state interaction, fits the experimental results better than line shapes based on the JDOS model of critical points. As an example, in Fig. 8 we show a comparison between the second derivative of the dielectric function calculated from the experimental data for the SL in the vicinity of the major part of the  $E'_1$  structure, and the fits according to both the two-dimensional critical-point line shape and the Lorentzian profile. Even for this interband transition far above the fundamental edge a clear deviation from the model of pure two- or three-dimensional critical points is observed.

TABLE I. Interband transition energies of the characteristic critical points for the superlattice and the bulk samples at  $T=90$  K. For the superlattice the assignment of transitions to locations in the BZ means the related and folded points.

	GaAs	AlAs	SL
$E_1(P_1)$	2.846	3.892	3.015
	2.929	3.943	3.120
	3.010	3.987	3.220
	3.079	4.053	3.300
	3.150	4.103	3.399
$E_1 + \Delta_1(P_1)$	3.221	4.156	3.499
$E'_0(\Gamma - \Delta)$	4.477		
	4.638		
	4.767		
$E_2(X)$	4.888	4.622	4.679
		4.717	4.769
$E_2(\Sigma)$		4.846	4.871
$E_2(P_2)$	5.068	4.929	4.953
$E'_1(P'_1)$	6.578	6.475	6.470
$E'_1(L)$	6.895	6.810	6.975
<b>Ga 3d</b>			
$j = \frac{5}{2} (L)$	20.266		20.272
$j = \frac{5}{2} (X)$	20.463		20.468
$j = \frac{3}{2} (L)$	20.695		20.743
$j = \frac{3}{2} (X)$	20.909		20.926

## V. DISCUSSION

### A. Ga 3d transitions

We first discuss transitions from the core levels. As known from band-structure calculations which consider the  $d$  electrons as not belonging to the fixed ion core,<sup>28</sup> the Ga 3d levels exhibit virtually no dispersion throughout the BZ. Moreover, x-ray-photoemission spectroscopy (XPS) measurements have not revealed chemical shifts for the Ga 3d core levels between bulk GaAs and GaAs/AlAs superlattices.<sup>29,30</sup> For this reason they represent an ideal energy reference which can be used to measure the energy positions of the CB via optical interband transitions. This method will be useful in separating the confinement and splitting effects for the VB and CB in the case of a heterostructure.

Since the Ga 3d levels are quasidispersionless,  $\nabla_{\mathbf{k}} E_{\text{core}}(\mathbf{k})$  is zero. Therefore, with Eq. (3), the density of states of the CB,  $J_c$ , rather than the JDOS,  $J_{\text{core},c}$ , governs the optical transitions. For excitations from these core levels the dipole approximation is still appropriate. The wavelength of light is about 70 nm at 20 eV in the material. Thus the wavelength of light is still large compared to the size of the 3d wave functions, which are strongly localized around the Ga site. However, an appropriate large- $\mathbf{k}$  interval is needed to represent these wave functions in  $\mathbf{k}$  space. For this reason  $\mathbf{k}$  no longer remains a good quantum number to represent such localized states.

The  $f$ -sum rule for the oscillator strength<sup>31</sup>

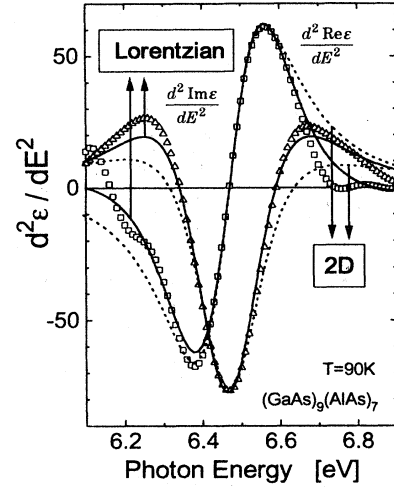


FIG. 8. Comparison between the two-dimensional line shape within the JDOS model of critical points (dashed lines) and the Lorentzian (solid lines), applied to experimental values of the real (squares) and imaginary (triangles) parts of the second derivative of the dielectric function in the vicinity of the major part of the  $E'_1$  structure for the  $(\text{GaAs})_9(\text{AlAs})_7$  superlattice. Similar line shapes also appear in the case of the GaAs and AlAs bulk samples.

$$\int_0^\infty \omega \epsilon_2(\omega) d\omega = \frac{\pi}{2} \omega_p^2 \quad (6)$$

can be transformed into an expression which to a good approximation gives the number of excited electrons per atom,  $N_{\text{eff}}$ :

$$N_{\text{eff}}(E) = \frac{2}{\pi} \frac{\epsilon_0 m}{\hbar^2 e^2} \frac{a_L^3}{N_U} \int_{E_0}^E E' \epsilon_2(E') dE', \quad (7)$$

where  $E = \hbar\omega$  is the photon energy,  $E_0$  the energy of the fundamental absorption edge,  $N_U$  the number of atoms per unit cell,  $a_L$  the lattice constant,  $m$  the electron mass, and  $\epsilon_0$  the dielectric permittivity of the vacuum. The evaluation of this integral reveals (Fig. 9) that the VB oscillator strength for GaAs is exhausted at  $N_{\text{eff}} \approx 3.5$  near 20 eV. For AlAs the sum rule exhibits some saturation

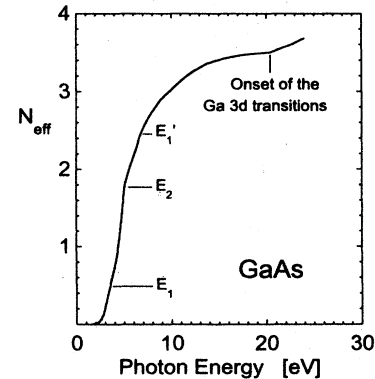


FIG. 9. Sum rule evaluation for GaAs showing the exhaustion of the VB oscillator strength until 20 eV, and the onset of transitions from the Ga 3d levels to the lower conduction-band minima.

around 11 eV followed by a weak, nearly linear increase. No additional structure above this energy up to 25 eV is found in the spectrum of the dielectric function for AlAs, in contrast to GaAs, where a sharp bend in the integrated oscillator strength at an energy of 20 eV is accompanied by two broad structures in the dielectric function (Fig. 7).

These structures in the GaAs spectra above 20 eV must be due to excitations from core levels. For Ga, these are the 3*d* levels, for Al the 2*p*, and for As the 3*d* levels. Because structures are observed for GaAs but not for AlAs, their origin should be due to the Ga 3*d* levels. Experimental XPS data<sup>29,30</sup> indicate binding energies relative to the top VB edge of 18.75±0.03, 72.7±0.05, and 40.74 eV for the Ga 3*d*, Al 2*p*, and As 3*d*, respectively. Taking into account the corresponding fundamental gap, the two peaks observed in the energy range between 20 and 25 eV in the imaginary part of the dielectric function for GaAs originates clearly from transitions from the Ga 3*d* levels to the CB. The important part of this spectrum consists of the onset of the first peak, which marks the transition from the Ga 3*d* levels to the CB minima which are lowest in energy. Therefore structures in this region correspond to transitions to either the  $\Gamma_1^c$ ,  $X_1^c$ ,  $X_3^c$ , or  $L_1^c$  minimum. In previous works the relative strengths of these transitions were calculated taking into account the JDOS and the interband matrix elements.<sup>32,33</sup> It turned out that the  $X_3^c$ - and  $\Gamma_1^c$ -related transitions are very weak, and the strength of the  $L_1^c$ -related transitions should be smaller than the  $X_1^c$ -related ones. The now-accepted ordering of the CB minima,  $\Gamma$ - $L$ - $X$  with increasing energy, was first clarified by Aspnes.<sup>34</sup> We thus assign the first two of the four main contributions, which are indicated as minima in the second derivative of the dielectric function vs photon energy, to transitions from the Ga 3*d* level ( $j = \frac{5}{2}$ ) to the  $L$  and  $X$  minima of the CB in the order of increasing energy. The higher two minima correspond to their spin-orbit-split counterparts ( $j = \frac{3}{2}$ ). For the SL we found similar transitions as in the case of GaAs, revealing virtually no effect of the superlattice potential on the lowest CB at  $L$ - and  $X$ -related points [Fig. 4(A2)].

Before applying the line-shape analysis to the experimental data, we have to recognize that the dielectric function in the region of the Ga 3*d* excitations consists of two parts: (a) the actual contribution from the Ga 3*d* excitations, and (b) the superimposed Drude contribution originating from the VB electrons. The latter contribution must be subtracted from the dielectric function data to obtain the true line shapes according to the core-level transitions. This will be attained by representing the entire VB-CB transitions as a harmonic-oscillator resonance near the energy position of the main  $E_2$  structure, and modeling with it the shape of the measured dielectric function between the plasma resonance at about 15 eV and the onset of the Ga 3*d* excitations at 20 eV.

The evaluation of the Ga 3*d* line shapes reveals that the Lorentzian works better as compared to two- and three-dimensional line shapes for both GaAs and the (GaAs)<sub>9</sub>(AlAs)<sub>7</sub> SL. But a conclusion about the existence of 3*d* core excitons<sup>35–37,38,18</sup> seems to be difficult. No discrete exciton series has been observed until now in the Ga 3*d* core region. This could be explained by the rela-

tively large broadening compared to the exciton binding energy. For GaAs, the latter value was estimated by Aspnes<sup>35</sup> in the case of the Ga 3*d* to  $X_1^c$  transition to 90±250 meV in the following way: The energy difference between the core levels and the VB edge was determined by photoemission.<sup>38</sup> The addition of the fundamental gap resulted in a value which was larger than that estimated by core to CB minima transitions from optical experiments (electroreflectance,<sup>34</sup> energy-derivative reflectance<sup>36</sup>). The difference was then assigned to an exciton binding energy.

However, photoemission and optical data are difficult to compare since the sample probing depth is very different in the two cases. From the dielectric function data it follows that the penetration depth of light in the onset region of the Ga 3*d* transitions is about 50–500 lattice constants (Figs. 10 and 11). In contrast, for the energy range from 20 to about 200 eV the escape depth of a photoemitted electron reaches a minimum value, between one and two lattice constants. Therefore such photoemission data represent the properties of the outermost surface region of the sample. However, it is known that the fundamental gap of an unrelaxed, polar surface is smaller than that of the bulk.<sup>39</sup> The latter effect arises from surface states, resulting in a finite density of states in the gap below the CB and above the VB. This leads to an enlargement of the core-to-VB-edge distance. Furthermore, there exists a *surface* core-level shift of the Ga 3*d* levels to higher binding energies (Ref. 29). Thus core-to-CB-minima energy differences estimated by photoemission can be larger than the optical ones, which is due simply to the difference in surface and bulk properties. In conclusion, there seems to be no doubt about the occurrence of final-state interaction due to the core hole potential,<sup>37</sup> but so far there is no clear evidence of *discrete* states in the case of core-to-CB transitions.

### B. $E_1$ and $E_1 + \Delta_1$ transitions

$E_1$  and  $E_1 + \Delta_1$  structures are known to result from transitions from the uppermost spin-orbit-split VB to the

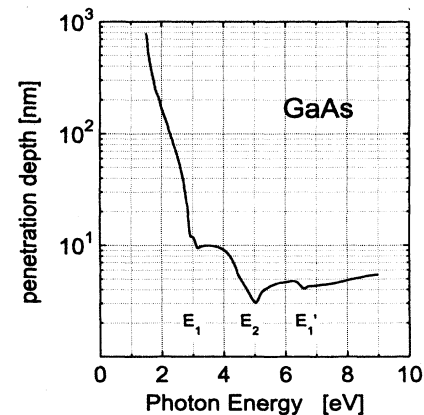


FIG. 10. Penetration depth of light in the photon energy range within the three main structures  $E_1$ ,  $E_2$ , and  $E_1'$ , determined for GaAs, indicating the importance of sample surface preparation too.

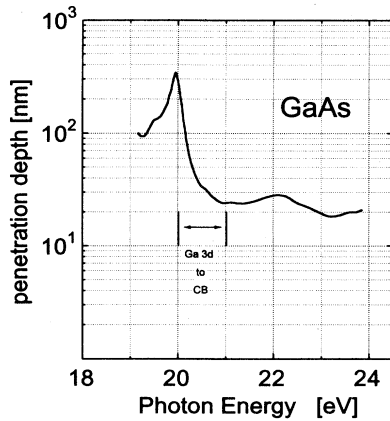


FIG. 11. Penetration depth of light vs photon energy for GaAs for the transitions from the Ga 3d levels to the lower conduction bands.

lowest CB near the  $L$  point along the  $\Lambda$  line in the BZ (Fig. 2). However, a region  $P_1$  in the  $\Gamma LK$  plane [Fig. 12(a)], where the bands are parallel, was also found to contribute to these critical points in GaAs.<sup>40</sup> Likewise the  $E_2$  structure originates mainly from such a BZ region ( $P_2$ ), located in the  $\Gamma XUL$  plane [Fig. 12(b)], which was derived from band-structure calculations for Si,<sup>41–43</sup> Ge,<sup>44,45</sup> GaAs,<sup>40</sup> and other III-V compounds. This confirms the assumption that the major structures in the dielectric function are not simply due to a single singularity in the JDOS at a high-symmetry  $k$  point or a restricted  $k$  interval on a symmetry line but rather due to relatively extended regions in the BZ. It reveals the difficulties in extracting a definite symmetry for critical points by appropriate experiments with symmetry-lowering perturbations. If large contributions could

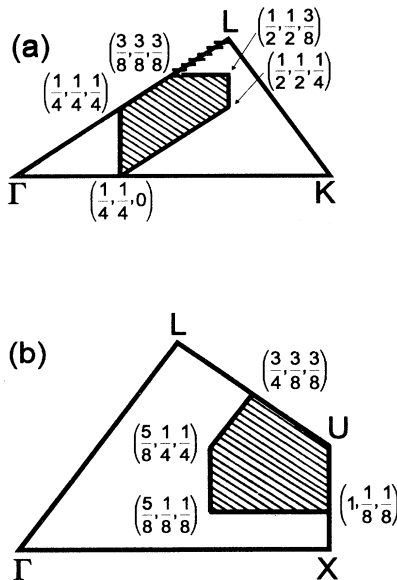


FIG. 12. Regions of special  $k$  planes in the zinc-blende Brillouin zone which contribute to (a) the  $E_1$  and (b) the  $E_2$  critical-point structures of GaAs (Ref. 40).

come from regions of no high symmetry, one fails to assign the structures to a certain symmetry point or line. Thus calculations are desirable which also reveal the JDOS off the high symmetry lines.

For the bulk materials GaAs and AlAs, the  $E_1$  structure consists of two major peaks (Fig. 3) which are due to the spin-orbit splitting on the VB along  $\Lambda$ . We estimate the magnitude of this spin-orbit splitting,  $\Delta_1$ , to 0.211 eV for GaAs, and to 0.169 eV for AlAs.

In our investigation we have resolved that both the  $E_1$  and  $E_1 + \Delta_1$  transitions consist of a threefold structure for GaAs and AlAs. Each of these two structures exhibit a main peak accompanied by two weak shoulders at its low-energy side. All three contributions of each structure are well distinguished as minima in the second derivative spectra (Fig. 4). Similar results were obtained using cleaved (110)GaAs samples.

The fact that these features were not seen in former investigations using samples with less perfect surfaces indicates their possible origin. The observed structures may be due to interband transitions between bent bands in the surface region. This assumption is supported by the fact that the additional structures appear at the low-energy side of the major peaks, and that the penetration depth of light approaches 10 nm at the  $E_1$  structure (Fig. 10). Recently Kuball *et al.*<sup>46</sup> found a distinct peak below the  $E_1$  critical point at 2.75 eV by investigating cleaved GaAs samples under vacuum conditions. They attributed this peak to electronic transitions at the surface because it vanishes with hydrogen exposure. Another reasonable explanation for the additional shoulders may be different origins in  $k$  space for the  $E_1$  structure. Critical points at  $L$ , along  $\Lambda$  (Ref. 19) and in the  $\Gamma LK$  plane, should have different interband energies. Thus  $E_1$  and  $E_1 + \Delta_1$  structures can exhibit a splitting according to these contributions.

Considering the corresponding transitions in the case of the SL, we have found two spin-orbit-split groups of three transitions, but they are shifted by more than 200 meV to higher energies compared to the GaAs  $E_1$  structure. It should be emphasized that no additional splitting due to the SL potential is observed for the SL  $E_1$  structure.

Figure 1 reveals that for GaAs the CB energy is lower and the VB energy is higher compared to AlAs at the  $L$  point, and the interband spacing for AlAs is about 1 eV larger than for GaAs. Thus we can conclude that the  $E_1$  transition in the SL takes place mainly in the GaAs component, and that the observed blueshift is due to a confinement effect. However, in contrast to the picture of energy offsets between the bulk band structures of GaAs and AlAs (Fig. 1), the SL potential leads only to a confinement effect on the upper VB, since virtually no effect on the CB at  $L$  was found in the corresponding transitions from the Ga 3d levels.

The interpretation of the SL spectrum remains the same if we admit that the major  $E_1$  contribution arises from transitions off the  $L$  point, in the  $\Gamma LK$  plane of the GaAs component, since the latter is near  $L$ . If the difference between the energy dispersions of the respective bands of GaAs and AlAs is smaller than the

difference in their energy eigenvalues, the confinement will still be maintained.

### C. $E_2$ transitions

The  $E_2$  transitions of GaAs are assigned mainly to a region  $P_2$  of parallel bands within the  $\Gamma XUL$  plane in the BZ (Ref. 46) which spreads from  $U$  toward  $X$  and  $L$  [Fig. 12(b)]. In GaAs, the  $E_2$  structure overlaps in energy with the  $\Gamma$ - $\Delta$ -related  $E'_0$  transitions. The currently accepted assignment for GaAs (Refs. 23 and 47) attributes the structure below 4.5 eV (Fig. 5) to the  $E'_0$  critical point near  $\mathbf{k}=(0.1,0,0)$ . A study of the band structure in the vicinity of the  $\Gamma$  point using nonlocal pseudopotentials<sup>45</sup> reveals an energetical splitting  $\Delta'_0 \approx 170$  meV on the second-lowest CB at  $\Gamma$  and  $\Delta'_0 \approx 160$  meV on the uppermost VB in the  $\Delta$  direction. Therefore both transitions at  $\Gamma$  and along  $\Delta$  should contribute to the structure above 4.6 eV. The strong structure near 5.0 eV is assigned to critical points in the  $\Gamma XUL$  plane, and the structure at 4.9 eV to  $X'_{1,3}$ - $X''_{1,3}$  transitions.

For AlAs the assignment of structures to critical points is less certain. Ellipsometric investigations using an AlAs sample with a protective GaAs overlayer<sup>48</sup> yielded two strong contributions at 4.641 and 4.764 eV for  $T=80$  K which were attributed to the  $E'_0$  and  $E_2$  critical points in order of increasing energy. Likewise, by ellipsometric studies,<sup>47,49</sup> the dependence of the spectral positions of the critical-point energies with varying Al content was investigated using a series of  $\text{Al}_x\text{Ga}_{1-x}\text{As}$  samples including the endpoints GaAs and (cap protected) AlAs. In this study the two main structures of AlAs, which decrease in amplitude with decreasing Al content, were attributed to transitions from the spin-orbit-split VB to the lowest CB at  $X$ .

From band-structure calculations<sup>40,47</sup> (Fig. 1) one finds a tendency for more parallelism between the highest VB and the lowest CB along  $\Delta$ - $X$ - $\Sigma$  from GaAs to AlAs, leading to an increased JDOS for the corresponding  $E_2(X)$  and  $E_2(\Sigma)$  transitions. In contrast, in the vicinity of the  $\Gamma$  point the second-lowest CB and the highest VB become nonparallel from GaAs to AlAs, resulting in a decrease of the corresponding JDOS for the  $E'_0(\Gamma)$  excitation. This is consistent with the observed weakening of the  $E'_0$  transitions and the enhancement of the  $E_2(X)$  ones from GaAs to AlAs in the comparison of the GaAs- $\text{Al}_x\text{Ga}_{1-x}\text{As}$ -AlAs spectra. The splitting between the two main transitions in AlAs and in the  $(\text{GaAs})_9(\text{AlAs})_7$  SL is consistent with the splitting of the VB along  $\Delta$  to  $X$  which amounts to 100 meV.<sup>44</sup> Moreover, the evaluation of band-structure calculations<sup>47</sup> for AlAs reveals a weakening of the  $E_2(P_2)$  transition compared to GaAs because of matrix element effects. Additionally the  $E_2(\Sigma)$  critical point originating from a region around the  $K$  point<sup>47</sup> is separated from the  $E_2(P_2)$  structure by about 120 meV in the case of AlAs, in contrast to GaAs where these transitions are nearly degenerate in energy. Therefore we attribute the transition at 4.846 eV to the  $E_2(\Sigma)$  critical point and the structure at 4.929 eV to the  $E_2(P_2)$  one.

We found that the derivative spectrum of the SL in the vicinity of the  $E_2$  structure (Fig. 5) is AlAs like, and very different from that of GaAs. Therefore the corresponding SL transitions are assigned mainly to the AlAs component. Since the  $X$ -related Ga  $3d$  to CB minima transitions, taking place in the GaAs component of the SL, show no splitting or confinement effects, the energy of the lowest GaAs CB at  $X$  must be equal or higher compared to that of the AlAs one. If it is higher this would result in a confinement effect for those transitions at  $X$ , which are mainly in AlAs. From the band-structure calculations (Fig. 1) one can see that the energy difference between the lowest CB's of GaAs and AlAs has a finite value at  $X$ , decreasing to zero along  $\Delta$ . This agrees well with the experimental result of a blueshift for the SL structures compared to AlAs, and confirms the assignment of the AlAs  $E_2$  transitions to critical points near  $X$ .

In addition, a strong minimum in the derivative spectrum of the dielectric function for the SL at an energy of 4.953 eV was found and a weaker one at 4.871 eV which exhibits the same blueshift of 25 meV compared to the  $E_2(\Sigma)$  and  $E_2(P_2)$  transitions in AlAs, respectively. Band-structure calculations carried out comparatively for bulk and SL samples<sup>50</sup> attribute the strong structure<sup>8</sup> to a SL transition because a corresponding counterpart in the bulk spectra was not found. This additional structure was assigned in Ref. 50 to parallel band transitions along the  $\Gamma$ - $X$  direction and transitions between folded bands near  $\Gamma$ - $Z$ . However, our results suggest that this SL transition should correspond to the  $E_2(P_2)$  critical point in AlAs. This hypothesis is supported by the fact, that a similar structure between 4.9 and 5.0 eV was also observed in the  $\text{Al}_x\text{Ga}_{1-x}\text{As}$  spectra with  $x \approx 0.5 \dots 0.6$  in Ref. 47.

Moreover we note that in the vicinity of the  $E_2$  structure the second derivative spectra of the dielectric function for the  $(\text{GaAs})_9(\text{AlAs})_7$  SL and an  $\text{Al}_{0.5}\text{Ga}_{0.5}\text{As}$  alloy<sup>47</sup> looks qualitatively similar except for two basic differences. The broadening of the first of the two main SL structures is much smaller than that of the alloy, and the spectrum of the SL exhibits more fine structure on the high-energy side.

### D. $E'_1$ transitions

The  $E'_1$  structure of the investigated samples consists of two contributions, a major peak around 6.5 eV and a shoulder at its high-energy side (Fig. 6). LMTO band-structure calculations within the local-density approximation (LDA) (Ref. 40) (Fig. 1) place the  $E'_1$  structure just below 6 eV and assign it mainly to transitions along  $\Delta$ . However, LDA calculations underestimate the energy of the conduction bands, and hence the interband spacing. Other band-structure calculations using nonlocal pseudopotentials<sup>44</sup> leave it at the known tentative assignment of these transitions to  $L$ .<sup>51,52</sup> We found that the major  $E'_1$  peak for the SL is an AlAs-like transition (Fig. 4), and shows no confinement effect. Therefore the transition should take place mainly in the AlAs component.

From Fig. 1 one can infer that the energy eigenvalue

for the second-lowest CB of AlAs at  $L$  is lower than that of GaAs. The energy of the uppermost VB of AlAs at  $L$  is also lower than that of GaAs. Within the picture of energy offsets between the bulk band structures, if an  $L$ -related transition from the uppermost VB to the second-lowest CB takes place in the AlAs component of the SL, a confinement effect due to the CB has to occur. If the transition is in the GaAs component, we should observe a confinement effect due to the VB, as was really found by the investigation of the  $E_1$ -related transitions. However, no such effect is seen at all. This may be due to a folding of the energy bands along  $\Lambda$  which is neither parallel nor perpendicular to the growth direction. Otherwise the assignment of this transition to  $L$  would be questionable.

Unlike the major  $E_1'$  peak, the experimental spectra reveal a blueshift of the minor  $E_1'$  transition of 165 meV compared to the corresponding transition of AlAs, and of 80 meV compared to that of GaAs. Qualitatively this result is consistent with the confinement at  $L$  derived from the band structures, assuming in addition that the wave functions are distributed between the GaAs and AlAs components.

Since we have found a different confinement behavior for the two contributions of the  $E_1'$  structure, they cannot be assigned to the same  $\mathbf{k}$  location in the BZ. Consequently, the energy separation between the two parts of the  $E_1'$  structure does not have the meaning of a spin-orbit splitting. Otherwise this separation energy should be the same as the splitting of the  $E_1$ - and  $E_1 + \Delta_1$ -related transitions, too. However, we found values for the energy separation of the  $E_1'$ -related transitions which are about one and a half times as large as the  $E_1$ -related spin-orbit splitting.

Additional transitions are found on both the high- and low-energy sides of the  $E_1'$  structure in all samples (Fig. 6). For the bulk samples these structures are relatively broad and weak. The respective transitions in the SL are very weak and not well suited for line-shape analysis. Band-structure calculations<sup>45,40</sup> assign critical points in the energy range above the  $E_2$  and below the  $E_1'$  structures to transitions between the uppermost VB and the second-lowest CB along  $\Delta$  in the vicinity of the point  $\mathbf{k} = (0.55, 0, 0)$ . For AlAs we found corresponding transitions at 5.6/5.7 eV. GaAs exhibits a structure at 5.9 eV and the  $(\text{GaAs})_9(\text{AlAs})_7$  SL shows a very weak one near 6.0 eV.

Figure 3 has revealed that the major structures in the dielectric function are the  $E_1$ ,  $E_2$ , and  $E_1'$  ones. It was already pointed out that the  $E_1$  and  $E_2$  structures result largely from certain regions in the BZ where the bands

are parallel. This leads to the assumption that for the major  $E_1'$  contribution such a special region  $P_1'$  in the BZ should also exist. It would be desirable that band-structure calculations are performed which search explicitly for such regions making large contributions to the JDOS.

## VI. CONCLUSIONS

A comprehensive investigation of the optical properties of a short-period GaAs/AlAs superlattice and its bulk constituents has been performed over the wide range of photon energies  $3 \leq \hbar\omega \leq 25$  eV with the samples permanently under UHV conditions. The latter has the advantage of measuring samples with surfaces as grown, which guarantees the comparability of the results.

Spectroscopic ellipsometry using core levels for energy references has been shown to be a powerful tool to prove the band structure of bulk samples and heterostructures. The major structures  $E_1$ ,  $E_2$ , and  $E_1'$  of the dielectric function of the bulk samples and the Ga  $3d$  excitations of GaAs were also found for the SL. However, these structures are subject to particular changes due to the SL potential which results primarily in confinement effects and a spatial redistribution of the wave function to one of the components of the SL. Confinement effects could be separated for the various valence and conduction bands at  $L$ - and  $X$ -like points by the use of the Ga  $3d$  levels as an energy reference.

The precise determination of the differences between the corresponding transition energies of the investigated samples was realized by modeling the experimentally determined dielectric functions using the line-shape model of Eq. (5). A deviation from two- or three-dimensional line shapes as well as from the one-electron picture was found even for interband transitions far above the fundamental absorption threshold.

## ACKNOWLEDGMENTS

We express our appreciation to T. Buslaps and R. L. Johnson for their help concerning the UHV transport system, M. Hörnicke from the MBE group for the assistance in preparing the samples, and the staff of the synchrotron radiation center BESSY I for the technical support. Also, we would like to thank E. Jahne for a critical reading of the manuscript and helpful discussions. This work was partially supported by the German Federal Department of Research and Technology (BMFT) under Contract No. 05-5ESCAB9.

<sup>1</sup>W. Ge, W. D. Schmidt, M. D. Sturge, L. N. Pfeiffer, and K. W. West, *J. Lumin.* **59**, 163 (1994).

<sup>2</sup>H. Fujimoto, C. Hamaguchi, T. Nakazawa, K. Taniguchi, and K. Imanishi, *Phys. Rev. B* **41**, 7593 (1990).

<sup>3</sup>H. Kamimura and G. Shibata, *Jpn. J. Appl. Phys. Suppl.* **32-1**, 57 (1992).

<sup>4</sup>J.-B. Xia and Y.-C. Chang, *Phys. Rev. B* **42**, 1781 (1990).

<sup>5</sup>D. E. Aspnes and A. A. Studna, *Phys. Rev. B* **27**, 985 (1983).

<sup>6</sup>L. Vina, S. Logothetidis, and M. Cardona, *Phys. Rev. B* **30**, 1979 (1984); P. Lautenschlager, M. Garriga, L. Vina, and M. Cardona, *ibid.* **36**, 4821 (1987).

<sup>7</sup>M. Garriga, M. Cardona, N. E. Christensen, P. Lautenschlager, T. Isu, and K. Ploog, *Phys. Rev. B* **36**, 3254 (1987).

<sup>8</sup>U. Schmid, N. E. Christensen, M. Cardona, F. Lukes, and K. Ploog, *Phys. Rev. B* **45**, 3546 (1992).

<sup>9</sup>J. Barth, R. L. Johnson, and M. Cardona, *Phys. Rev. B* **41**,

- 3291 (1990).
- <sup>10</sup>C. Janowitz, O. Günther, G. Jungk, R. L. Johnson, P. V. Santos, M. Cardona, W. Faschinger, and H. Sitter, *Phys. Rev. B* **50**, 2181 (1994).
- <sup>11</sup>L. J. Sham and Y. T. Lu, *J. Lumin.* **44**, 207 (1989).
- <sup>12</sup>Y. T. Lu and Sham, *Phys. Rev. B* **40**, 5567 (1989).
- <sup>13</sup>M. C. Munoz, V. R. Velasco, and F. Garcia-Moliner, *Phys. Rev. B* **39**, 1786 (1989).
- <sup>14</sup>E. Ghahramani, D. J. Moss, and J. E. Sipe, *Phys. Rev. B* **43**, 9269 (1991).
- <sup>15</sup>G. Martinez, in *Handbook of Semiconductors*, edited by T. S. Moss and M. Balkanski (North-Holland, Amsterdam, 1980), Vol. 2, Chap. 4C, p. 186.
- <sup>16</sup>C. C. Kim, J. W. Garland, H. Abad, and P. M. Raccach, *Phys. Rev. B* **45**, 11 749 (1992).
- <sup>17</sup>L. van Hove, *Phys. Rev.* **89**, 1189 (1953).
- <sup>18</sup>F. Bassani and M. Altarelli, in *Handbook on Synchrotron Radiation*, edited by E.-E. Koch (North-Holland, Amsterdam, 1983), Vol. 1, Chap. 7, p. 534.
- <sup>19</sup>M. Cardona, *Modulation Spectroscopy* (Academic, New York, 1969).
- <sup>20</sup>D. E. Aspnes and A. A. Studna, *Phys. Rev. B* **7**, 4605 (1973).
- <sup>21</sup>R. M. A. Azzam and N. M. Bashara, *Ellipsometry and Polarized Light* (North-Holland, Amsterdam, 1987), p. 274.
- <sup>22</sup>D. E. Aspnes, in *Handbook of Semiconductors* (Ref. 15), Vol. 2, Chap. 4A, p. 110.
- <sup>23</sup>P. Lautenschlager, M. Garriga, S. Logothetidis, and M. Cardona, *Phys. Rev. B* **35**, 9174 (1987).
- <sup>24</sup>Y. Toyozawa, M. Inoue, T. Inui, M. Okazaki, and E. Hanamura, *J. Phys. Soc. Jpn.* **22**, 1337 (1967); M. Okazaki, M. Inoue, Y. Toyozawa, T. Inui, and E. Hanamura, *ibid.* **22**, 1349 (1967).
- <sup>25</sup>R. L. Johnson, J. Barth, M. Cardona, D. Fuchs, and A. M. Bradshaw, *Nucl. Instrum. Methods Phys. Res. Sect. A* **290**, 606 (1990).
- <sup>26</sup>J. Barth, R. L. Johnson, and M. Cardona, in *Handbook of the Optical Constants of Solids II*, edited by E. D. Palik (Academic, New York, 1991), pp. 213–246.
- <sup>27</sup>M. Cardona, *J. Phys. Chem. Solids* **17**, 336 (1961); *J. Appl. Phys.* **32**, 2151 (1961); M. Cardona and D. L. Greenaway, *Phys. Rev.* **131**, 98 (1963).
- <sup>28</sup>G. B. Bachelet and N. E. Christensen, *Phys. Rev. B* **31**, 879 (1985).
- <sup>29</sup>J. R. Waldrop, R. W. Grant, and E. A. Kraut, *J. Vac. Sci. Technol. B* **5**, 1209 (1987); E. A. Kraut, R. W. Grant, J. R. Waldrop, and S. P. Kowalczyk, *Phys. Rev. B* **28**, 1965 (1983).
- <sup>30</sup>E. T. Yu, D. H. Chow, and T. C. McGill, *Phys. Rev. B* **38**, 12 764 (1988).
- <sup>31</sup>D. Y. Smith, in *Handbook of the Optical Constants of Solids*, 2nd ed., edited by E. D. Palik (Academic, New York, 1986), pp. 35–68.
- <sup>32</sup>D. E. Aspnes, *Phys. Rev. B* **12**, 2527 (1975).
- <sup>33</sup>P. Thiry, Y. Petroff, R. Pinchaux, J. R. Chelikowski, and M. L. Cohen, *Solid State Commun.* **20**, 1107 (1976).
- <sup>34</sup>D. E. Aspnes, *Phys. Rev. B* **14**, 5331 (1976).
- <sup>35</sup>D. E. Aspnes, in *Festkörperprobleme XVII*, edited by J. Treusch (Vieweg, Braunschweig, 1977), p. 246.
- <sup>36</sup>D. E. Aspnes, M. Cardona, V. Saile, M. Skibowski, and G. Sprüssel, *Solid State Commun.* **31**, 99 (1979).
- <sup>37</sup>S. M. Kelso, D. E. Aspnes, C. G. Olson, D. W. Lynch, and D. Finn, *Phys. Rev. Lett.* **45**, 1032 (1980).
- <sup>38</sup>L. Ley, R. A. Pollack, F. R. McFeely, S. P. Kowalczyk, and D. A. Shirley, *Phys. Rev. B* **9**, 600 (1974).
- <sup>39</sup>C. W. Wilmsen, *Physics and Chemistry of III-V Compound Semiconductor Interfaces* (Plenum, New York, 1985).
- <sup>40</sup>M. Alouani, L. Brey, and N. E. Christensen, *Phys. Rev. B* **37**, 1167 (1988).
- <sup>41</sup>D. Brust, *Phys. Rev.* **139**, A489 (1965).
- <sup>42</sup>E. O. Kane, *Phys. Rev.* **146**, 558 (1966).
- <sup>43</sup>L. R. Saravia and D. Brust, *Phys. Rev.* **171**, 916 (1968).
- <sup>44</sup>M. L. Cohen and J. R. Chelikowski, *Phys. Rev. B* **14**, 556 (1976).
- <sup>45</sup>M. L. Cohen and J. R. Chelikowski, *Electronic Structure and Optical Properties of Solids* (Springer, Berlin, 1988).
- <sup>46</sup>M. Kuball, M. K. Kelly, P. V. Santos, and M. Cardona, *Phys. Rev. B* **50**, 8609 (1994).
- <sup>47</sup>S. Logothetidis, M. Alouani, M. Garriga, and M. Cardona, *Phys. Rev. B* **41**, 2959 (1990).
- <sup>48</sup>M. Garriga, P. Lautenschlager, M. Cardona, and K. Ploog, *Solid State Commun.* **61**, 157 (1987).
- <sup>49</sup>S. Logothetidis, M. Cardona, and M. Garriga, *Phys. Rev. B* **43**, 11 950 (1991).
- <sup>50</sup>M. Alouani, S. Gopalan, M. Garriga, and N. E. Christensen, *Phys. Rev. Lett.* **61**, 1643 (1988).
- <sup>51</sup>D. E. Aspnes, *Phys. Rev. Lett.* **33**, 1605 (1974).